ARTICLE OPEN



Long-term interactive corrosion between International Simple Glass and stainless steel

The interactive corrosion between stainless steel 316 (SS) and International Simple Glass (ISG) has been studied for 12 months. The samples were placed in intimate contact to create crevice corrosion conditions on SS in a 0.6 M NaCl solution with and without 142 ppm dissolved silica species enriched in ²⁹Si. Corrosion on SS was observed with large pits located close to the crevice mouth at the end of 1 year in 0.6 M NaCl solution. The SS corrosion was also associated with the dissolution of nearby glass in a highly localized manner. When the leaching solution was saturated with silica species, the corrosion rate of SS was suppressed. However, the presence of SS enhances ISG dissolution in both conditions. The implications of the observed phenomena on the long-term storage of nuclear waste are discussed.

npj Materials Degradation (2022)6:50; https://doi.org/10.1038/s41529-022-00262-0

INTRODUCTION

Borosilicate glasses are a suitable candidate host for disposal of high-level waste (HLW) due to its durability, the capability to vitrify various compositions of radionuclides in the glass matrix without crystallization of the glass, and ease of processing 1-4. The current plan in the U.S. and several other countries is to melt the glass-forming materials with the radionuclides beyond the glass transition temperature and cast the melt into stainless steel (SS) canisters. A large body of literature has been devoted to studying the dissolution mechanisms of waste glass forms and model waste glasses in chemically inert containers 5-8. However, the effects of near-field materials such as SS on the glass degradation need to be considered 9,10.

The effects of ferrous materials (iron metal and iron oxides and hydroxides) on the durability of borosilicate glasses have been studied. The first notable investigation was on the effects of Fe on borosilicate glass (labeled as PNL 76-68) by McVay and Buckwalter¹¹ who reported an enhancement of glass corrosion due to the precipitation of iron-silicate corrosion products, which removed silicate species from the solution, thus preventing solution saturation. Recently, Carriere et al. 12 observed that SON 68 glass alteration with iron led to the preferential precipitation of nontronite over a passivating gel with the glass dissolution occurring by dissolution/precipitation. In addition to secondary silicate phase precipitation, silicate species in solution can adsorb onto the surface of Fe oxides and cause a delay in saturation of the solution with respect to silica concentration. Secondary precipitation and adsorption have been broadly accepted as the mechanisms of enhanced glass corrosion in the presence of Fe and its oxides, although there seems to be some evidence that sorption of silicate species may be limited by site availability^{13,14}. However, some open questions remain about the characteristics of this mechanism. Oxidizing environments enhance the effect of Fe₃O₄ on glass corrosion by oxidation of Fe²⁺ to Fe³⁺, which has higher adsorption capacity for Si than Fe²⁺¹⁵, but glass corrosion may also be accelerated by Fe(OH)₃ in anoxic conditions¹⁶. Berger et al.¹⁷ showed that the incorporation of Fe in the gel layer on corroded glass depends on the distance between the reacting materials, suggesting metal cations can diffuse into the still-forming gel and the glass gel may be embedded with secondary precipitates.

In the planned repositories of several countries, such as the U.S., France, and Belgium¹⁰, the primary candidate canister material is SS, which is a corrosion-resistant alloy but highly prone to localized corrosion in the form of pitting and crevice corrosion. These forms of corrosion, once initiated, can propagate more rapidly than general corrosion¹⁸. SS dissolution might rapidly release a very high amount of metal cations in the solution that can precipitate with silicates. Woodland et al. 19 studied the effect of SS304 on the corrosion of simulated waste glass. The elemental release from the glass was doubled by the SS and alteration precipitates were observed. However, conditions for crevice corrosion like tight crevices was not mimicked in that study, so their result is likely associated with the uniform corrosion of SS. Pan et al.²⁰ investigated the effect of aqueous Fe²⁺ and Fe³⁺ (from FeCl₂ and FeCl₃, respectively) on model waste glasses and reported an increase of up to 50× in the corrosion rate of glass due to the enhanced acidity. Although the testing environment was a surrogate for a crevice due to the Fe cation hydrolysis and resulting low pH, they did not consider mass transport effects. Recently Guo et al.^{21,22} conducted studies to mimic aggressive conditions for crevice corrosion by placing the reacting borosilicate glass (International Simple Glass, ISG) in close contact with SS 316 and other corrosion-resistant alloys in Cl⁻ containing solutions. Crevice corrosion on SS 316 was observed along with increased ISG corrosion. The corrosion of ISG was aggravated in the contact region with SS (the crevice region) due to low pH conditions that originated from metal cation hydrolysis. On the other hand, the pH was alkaline outside the crevice due to the cathodic oxygen reduction reaction on the SS. Glass corrosion was enhanced there because the local high pH facilitated Si-O bond

¹Department of Materials Science and Engineering, The Ohio State University, Columbus, OH 43210, US. ²Department of Chemical Engineering and Materials Research Institute, Pennsylvania State University, University Park, PA 16802, US. ³CEA, DE2D, University of Montpellier, Marcoule, F-30207 Bagnols sur Cèze, 34000 Montpellier, France. ⁴Department of Mechanical Aerospace and Nuclear Engineering, Rensselaer Polytechnic Institute, Troy, NY 12180, US. ⁵Department of Geology and Geophysics, Louisiana State University, Baton Rouge, LA 70803, US. [≤]email: frankel.10@osu.edu



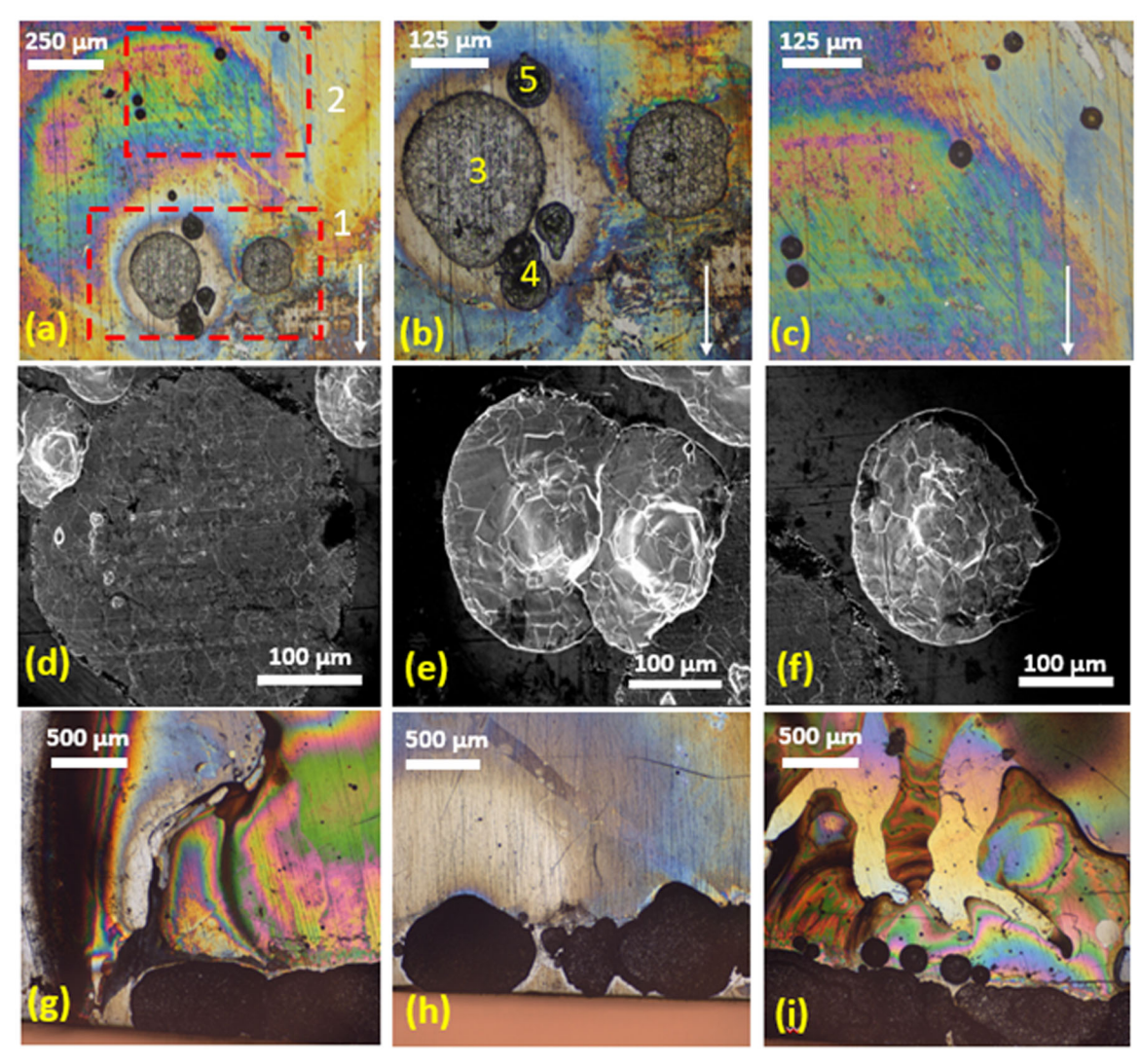


Fig. 1 Morphology of crevice corrosion observed on SS(+ISG) in 0.6 M NaCl after 12 months of exposure. a An optical microscopy image of SS(+ISG). The optical micrograph of regions 1 and 2 bounded by the red boxes are shown in (b) and (c) respectively. The white arrow is in the direction of the crevice mouth which is not visible in these images. d-f SEM (secondary electron) images of corrosion morphology observed. d corresponds to the pit numbered 3 in (b), (e) corresponds to the pit numbered 4 in (b) and (f) corresponds to the pit numbered 5 in (b), g-i Optical microscopy images of SS(+PTFE) showing extensive crevice corrosion.

hydrolysis. A protective silicate film formed on the SS surface, which slowed the crevice corrosion. Since the experiment was carried out for durations of up to 1 month, the nature of gel formation could not be assessed, especially if the reacting solutions were not previously saturated with SiO2. Low rates of passive dissolution of SS in SiO₂-containing solutions may still delay solution saturation. To gain better insight into such interactive corrosion, in this work ISG/SS samples were immersed in intimate contact in 0.6 M NaCl solution initially free of dissolved SiO₂ in the starting solution or saturated with soluble silica species (probably silicic acid or silicic ion), which will henceforth be referred to herein as SiO₂-saturated solution. Note that the concentration of 0.6 M NaCl solution corresponds to that of seawater and is the solution composition in the ASTM G 78 standard for crevice corrosion tests²³. This concentration may not be representative of that of a geologic repository but it is a reasonable test environment. Intimate contact was established by sandwiching an SS coupon between a pair of ISG coupons using polytetrafluoroethylene (PTFE) plates and PTFE nuts and bolts (see Fig. 11 in Methods). Both experiments were run for 1 year. All results were compared to control experiments where the SS was replaced with PTFE, which is inert in these environments, and so

only provides the geometric occlusion on the ISG with no added reactions. Samples of the solution were analyzed for elements from the glass and SS. The ISG samples were analyzed by Specular Reflectance Infrared (SR-IR) spectroscopy, Time of Flight Secondary Ion Mass Spectrometry (ToF-SIMS), X-ray Photoelectron Spectroscopy (XPS) and Scanning Electron Microscopy (SEM) of cross sections to evaluate the gel morphology.

RESULTS

Localized corrosion of stainless steel and ISG

The experimental groups are listed in Table 1. In the following discussions, the notation of X(+Y) is used, which describes the corrosion of material X exposed in close proximity to material Y. After one year of exposure in 0.6 M NaCl solution, severe localized corrosion was observed on SS(+ISG) (i.e., SS corroded in close proximity to ISG) in the form of large pits with a diameter of hundreds of micrometers (Fig. 1a–c). These pits were located approximately 1.5 mm away from the crevice mouth. This observation is consistent with the short-term results reported by Guo et al. 21,22 , who showed shallow localized crevice corrosion



Table 1. List of experimental groups and testing conditions used in the present study.								
Sample ID	Materials	NaCl Concentration (M)	Si concentration in starting solution (ppm)	Solution volume (mL)	SA/V (m ⁻¹)	Temperature (°C)	Duration (d)	
ISG(+SS)	ISG and SS 316	0.6	0	200	8.4	90	182, 365	
ISG(+PTFE)	ISG and PTFE	0.6	0	200	8.4	90	182, 365	
SS(+PTFE)	SS 316 and PTFE	0.6	0	200	8.4	90	182, 365	
ISG(+SS)	ISG and SS 316	0.6	141	50	33.6	90	30, 90, 182, 365	
ISG(+PTFE)	ISG and PTFE	0.6	141	50	33.6	90	30, 90, 182, 365	

near the crevice mouth but the degree of damage was less evident compared to what was observed in this study. The pits have coalesced and exhibit an etched-grain morphology (Fig. 1d-f) characteristic of activation-controlled dissolution²². The location of the damage being close to the crevice mouth is the consequence of heterogenous distribution of current density near the crevice mouth and the resulting ohmic potential drop²². It is worth noting that the amount of damage observed on SS is more substantial compared to what was reported by Guo et al.^{21,22}, who corroded SS in contact with ISG under similar conditions for a period of only 30 days. The site with the most damage was located farther away from the crevice mouth compared to the 30-day result, which is likely a consequence of the widening of the initial gap at the crevice mouth. Since the corrosion interaction between SS and glass is primarily driven by the aggressive environment created by localized corrosion of SS, the observation of more severe localized damage after a longer exposure time indicates that the interactive corrosion between SS and glass could be a long-lasting problem. Severe corrosion was observed on SS (+PTFE) as seen in Fig. 1g-i at the crevice mouth. Although glass corrosion products, such as silicates, can reduce the corrosion of SS by forming a layer of protective film²², this inhibitive effect is limited in this case and is clearly not sufficient to shut down the initiation or propagation of localized corrosion within the crevice formed by SS and ISG.

On the other hand, in 0.6 M NaCl solution saturated with SiO₂, the extent of localized attack on SS was much less, as is evident from optical micrographs shown in Fig. 2a–f. Only small and shallow pits are visible at the crevice mouth and center due to the inhibitive effect offered by dissolved silica. Pits of this scale are unlikely to create an environment as aggressive as exists in the crevice solution without pre-dissolved silica, so the degree of corrosion is much less for ISG(+SS) corroded in silica-saturated NaCl solution compared to ISG(+SS) corroded in NaCl solution without pre-dissolved silica. More details on the extent of glass alteration will be given in the following section.

When ISG was replaced with PTFE while keeping the surface area to solution volume (SA/V) ratio the same and testing in SiO₂saturated solution, localized attack was observed on SS in the creviced region. In the crevice mouth area, large pits with a dimension exceeding 100 µm are clearly visible (Fig. 2h), while only small pits exist at the crevice center as seen in (Fig. 2i). In silica-saturated condition, corrosion of SS was more evident with PTFE (Fig. 2g-i) than with ISG (Fig. 2a-f), implying that ISG dissolution impedes SS corrosion in addition to the inhibitive effect offered by dissolved silica. SEM images of SS(+ISG) taken at the crevice mouth (Fig. 3) show the precipitation of secondary phases. Chemical analysis of the precipitates by EDS indicates that they arise from the coprecipitation of ISG and SS corrosion products (Fig. 3b, d). The precipitation of such phases is much more evident in 0.6 M NaCl where the precipitates cover the SS substrate compared to that of SiO₂-saturated 0.6 M NaCl. This observation correlates with the extent of localized damage observed in Fig. 1, thus enforcing the idea that the corrosion interaction between SS and ISG is suppressed by the pre-dissolved silica in the electrolyte.

Figure 4a, b show optical profilometry images acquired on the ISG(+SS) sample exposed in 0.6 M NaCl solution and that of a pristine ISG sample, respectively. The surface of the ISG(+SS) sample is characterized by significant damage in the form of etching to depths of ~10 µm. Interestingly, the location of the attack region in Fig. 4a corresponds closely to the location of large pits on the contact area of the SS (Fig. 1a-c). This highly localized corrosion morphology on the ISG is due to the long-term influence of the aggressive environment created by the crevice corrosion of SS. Such an effect was not observed in the short-term study by Guo et al.^{21,22}. After being locally attacked, the glass corrosion products may combine with metal cations released from SS corrosion due to their high affinity²². Within the highly localized acidic environment, they are probably soluble, so they transport to the crevice mouth and precipitate along the path at locations near the crevice mouth where the pH increases. However, precipitation of glass corrosion product, particularly SiO₂, can also occur on the SS to create a partially protective film as observed by Guo et al.^{21,22}

Morphology of the alteration (gel) layer

Dissolution of alkali/alkaline boroaluminosilicate glasses leads to the formation of a porous and hydrated layer (gel layer) largely devoid of the mobile elements, viz. Na and B^{24,25}. In the absence of Si in the onset solution, gel formers (mainly Si and Al) partly dissolve, whereas in a silica-saturated solution, the gel keeps all Si and Al from the glass and reorganizes its structure after the release of mobile elements. The thickness of this gel layer is a measure of the extent of glass corrosion under a given condition and solution chemistry. The alteration layer thickness estimated from B release has been well correlated with the thicknesses measured by techniques such as spectroscopic ellipsometry and SEM²⁶. Thus, the samples of ISG(+SS) and ISG(+PTFE) were crosssectioned by slicing the glass along its length. The SS sample was therefore cut along its width horizontally while the glass is cut vertically. SEM images were acquired at different locations along the crevice length. In Fig. 5a, an SEM image acquired at the crevice mouth between an ISG and SS sample is shown. The gel thickness measured at a specific location is shown. An EDS line scan performed along the white line with the arrow pointing in the direction of the scan in Fig. 5a, is shown in Fig. 5b. The abrupt increase in the Na and Ca concentrations enable us to demarcate the gel from the bulk glass. Similar cross-section images of ISG (+SS) reacted in silica-saturated NaCl solution are shown in Supplementary Fig. 1. The thickness of the gel layer was $39 \pm 1 \,\mu m$ at the crevice mouth (Fig. 5a). The gel layer exhibits cracks that run transverse and longitudinal to the gel thickness. It is well known that structural reorganization leads to the formation of a stressed aluminosilicate gel layer due to an overall increase in the stiffness of the network resulting from the formation of higher polymerized



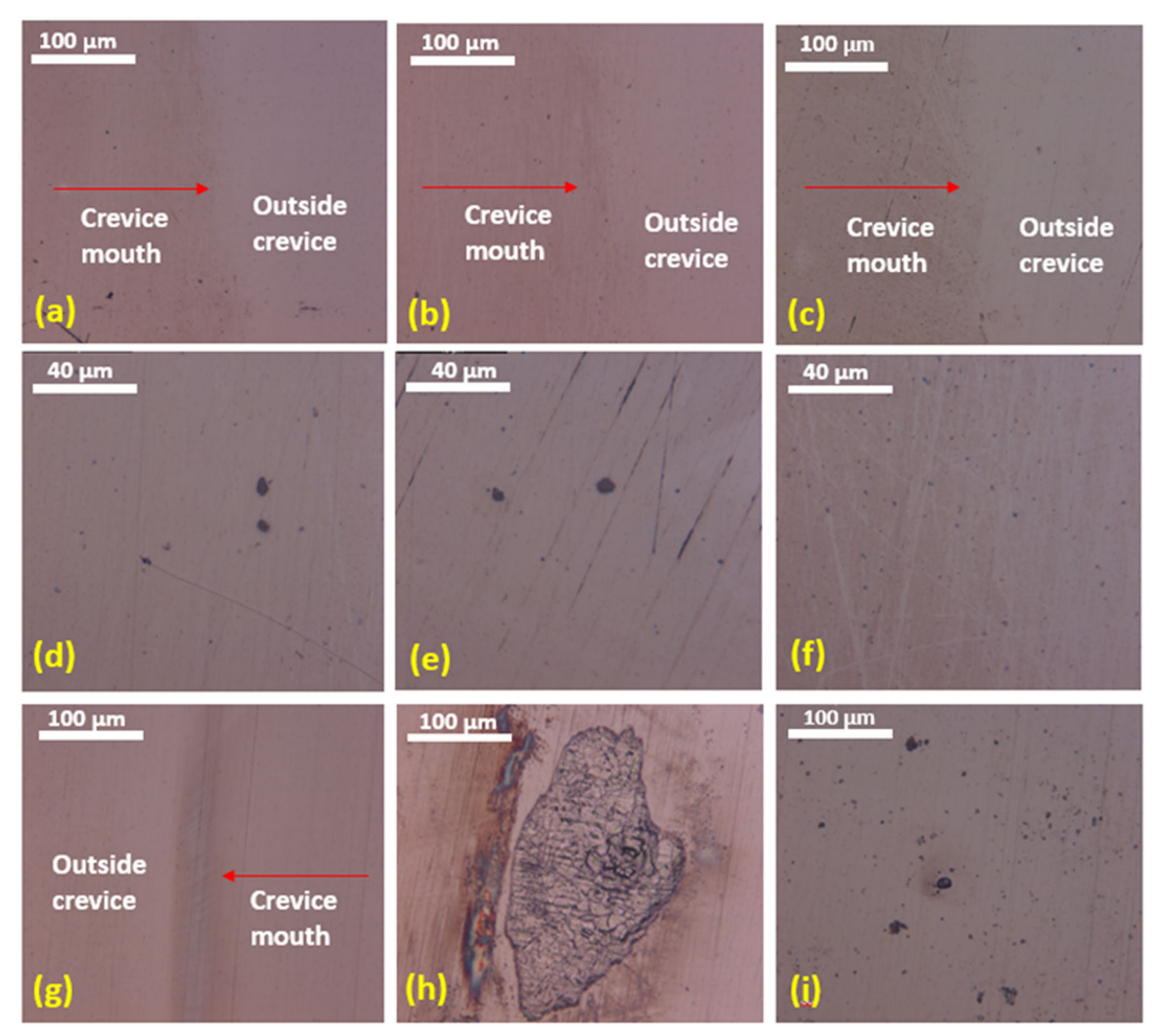


Fig. 2 Optical Microscopy images of morphology of crevice corrosion observed on SS(+ISG) and SS(+PTFE) after 12 months of exposure in silica-saturated 0.6 M NaCl. a-c Images acquired at the crevice mouth with arrows demarcating the crevice mouth. d-f Images acquired in the SS(+ISG) crevice interior. g-i SS(+PTFE).

silicate species^{21,27}. In addition to network stress, capillary forces from gel dehydration have shown to cause the formation of cracks in the gel layer probably during storage of samples after dissolution experiments²¹. However, cracks observed in the bulk of the glass specimen may have been a result of machining and polishing of the cross-sections since such cracks were not observed on the polished and uncorroded glass samples. The gel thickness variation as a function of distance into the crevice for 0.6 M NaCl and silica saturated solutions is shown in Fig. 5e. The decrease of the gel thickness with distance into the crevice is expected due to two reasons: 1) the presence of a more aggressive environment at the crevice mouth compared to the crevice center owing to the crevice corrosion of SS, and 2) a high SA/V and a low solution renewal rate inside the crevice center²⁸. The cross-section of ISG(+PTFE) exposed to 0.6 M NaCl exhibited a gel thickness of $29 \pm 1 \mu m$ at the crevice mouth, which is 25% less than ISG(+SS) reacted at identical SA/V ratio, as seen in Fig. 5c. This thickness decreased to $24 \pm 1 \mu m$ at 200 μm from the crevice mouth (Fig. 5d). For silica-saturated NaCl solution, the gel thickness at the crevice mouth is $3.35 \pm 0.05 \,\mu m$ and this thickness also decreased along the length of the crevice (Fig. S1a-d). Like the case of 0.6 M NaCl solution, the gel layer was thinner in the presence of an inert material like PTFE (Fig. S1e, f), although the difference is marginal. Since gel thickness is an indication of the

extent of glass corrosion, these observations demonstrate the enhancement of glass corrosion due to the presence of SS and the inhibitive effect of predissolved silica.

Solution analyses

The results of solution analyses for ISG(+SS) and ISG(+PTFE) in 0.6 M NaCl are shown in Supplementary Table 1. Normalized loss (NL) values are given in Fig. 6 for 0.6 M NaCl and Fig. 7 for silicasaturated NaCl. The data points at 30 days in Fig. 6 are results from the previous short-term study undertaken by Guo et al.²¹. In the solution without silica (Fig. 6), the NL values at 182 and 365 days are higher than those at 30 days for B, Ca and Si, as expected. For ISG(+SS), B apparently reached a plateau after six months of exposure in 0.6 M NaCl (Fig. 6a), the value of which is ~25% higher than that of ISG(+PTFE) corroded under similar conditions. The observation of B plateauing is consistent with the findings of Pan et al.²⁰, who corroded model nuclear waste glasses in highly acidic FeCl₃ solutions simulating the aggressive environment created by the localized corrosion of SS. Under such aggressive conditions, the release of B from the pristine glass into the leaching solution through the slowly growing gel layer is primarily controlled by diffusion and depolymerization of the silica network in the gel layer. The elevated NL values for B, Ca and Si for ISG(+SS) with respect to ISG(+PTFE) further validate the adverse effect of SS

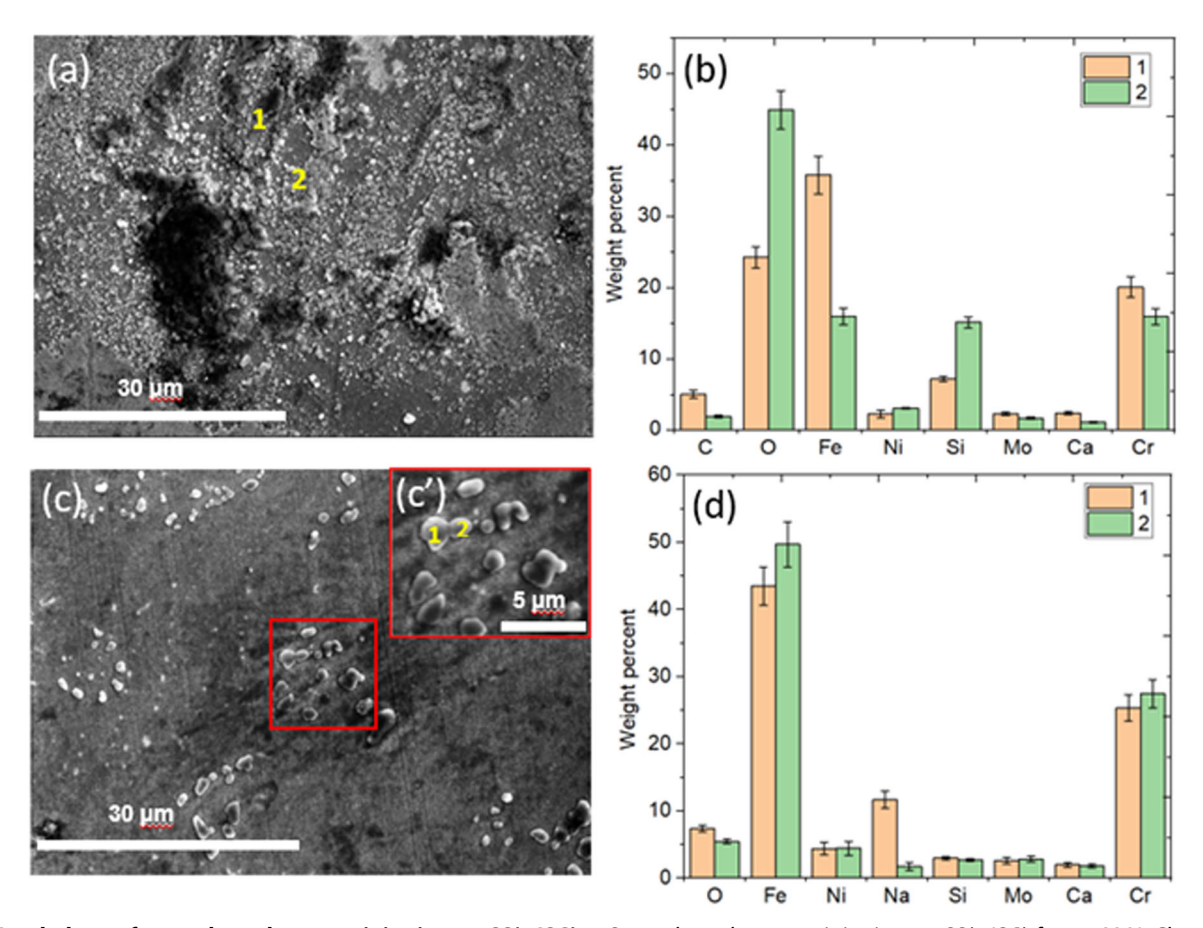


Fig. 3 Morphology of secondary phase precipitation on SS(+ISG). a Secondary phase precipitation on SS(+ISG) for 0.6 M NaCl outside the crevice mouth. b Chemical composition of precipitates determined at points 1 and 2 in (a). c Secondary phase precipitation on SS(+ISG) for silica-saturated NaCl outside the crevice mouth. d Chemical composition of precipitates determined at 2 regions (1 and 2 in inset c') by EDS.

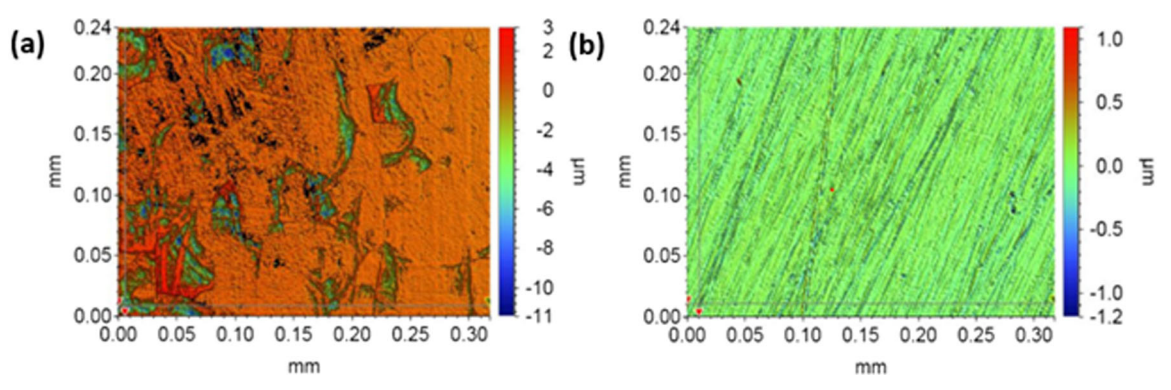


Fig. 4 Optical Profilometry of ISG. a Localized attack on ISG(+SS) corroded in 0.6 M NaCl. b Optical Profilometry of pristine ISG.

toward glass corrosion. However, it is probable that the data point for B corresponding to ISG(+PTFE) at 365 days (Fig. 6a) is an experimental artifact, because B is generally not involved in the precipitation of secondary phases. B adsorption has been observed on oxides of Fe²⁹ with the enhancement of adsorption kinetics in neutral to slightly alkaline pH range. However, in the presence of other Fe oxides like magnetite, no significant B adsorption has been observed³⁰. It is known that a higher oxidation state of Fe correlates with higher Si adsorption¹⁴. Therefore, it may be reasonable that B adsorption may also depend on the Fe oxidation state. Further studies are required to examine B adsorption on oxides of SS. Therefore, in such complex

systems, the utility of B as a tracer needs to be examined carefully. The morphological characterization shown in Fig. 4 shows that the adverse effect of SS on ISG corrosion is highly localized. In the short-term (30 days) study²¹, this local effect was dominated by the influence of the bulk solution, so it is surprising that the difference between the leaching solution of ISG(+SS) and ISG+(PTFE) is distinguishable for the long-term exposure. This further highlights the strong but local accelerating effect of SS on glass alteration. The decrease in the NL of Si and Ca after 1 year of exposure is probably due to the precipitation of secondary phases. This hypothesis is backed by the identification of widespread secondary phases existing on the surface of SS (Fig. 3). The large



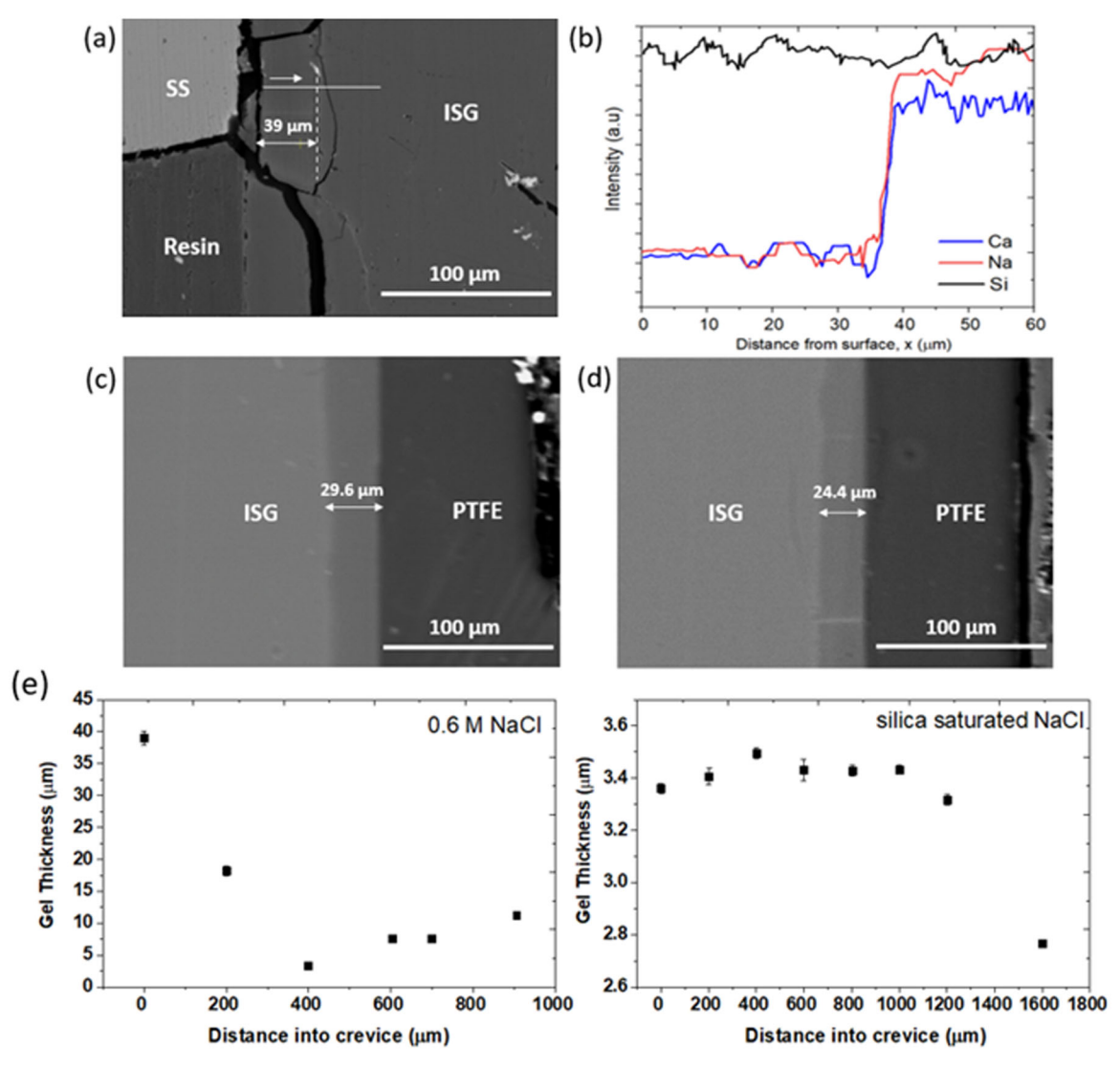


Fig. 5 SEM images of cross-sections of ISG(+SS) and ISG(+PTFE) reacted in 0.6 M NaCl for 1 year. ISG(+SS) cross-section images acquired at (a) at the crevice mouth. (b) An EDS line scan performed along the white line in (a) with the arrow pointing in the direction of the scan (c) ISG(+PTFE) cross-section image acquired at the crevice mouth. (d) ISG(+PTFE) cross section image acquired at 200 μ m into the crevice mouth. (e) The variation of gel layer thickness along the distance into the ISG(+SS) crevice for both 0.6 M NaCl and silica saturated NaCl solutions at the end of t=365 days of reaction.

decrease in Al concentration with respect to the 30 day data from Guo et al.²¹ (Fig. 6d) is probably due to the precipitation of aluminosilicates.

The solution analyses results for silica saturated NaCl solution are given in Table 2. The NL values of B, Ca and Si increase with time with no evidence of plateaus in the ISG(+SS) experiment as seen in Fig. 7a. However, the NL values of these three elements were approximately one order of magnitude lower compared to those measured in 0.6 M NaCl (Fig. 6), which is consistent with the smaller gel layer thickness measured by SEM (Fig. 5). Figure 7b shows the concentration of Si measured by ICP-MS over the entire duration of 365 days. A peculiar behavior was seen for the isotopic concentrations of Si. Between 0 and 30 days, the concentration of ²⁸Si decreased from 80.8 ppm to 21.1 ppm and the concentration of ²⁹Si decreased from 61.4 ppm to 42.1 ppm. This behavior is reflected in the ²⁹Si/²⁸Si isotopic ratio, which was 0.76 at the beginning of the experiment and 2 after 30 days, as seen in Fig. 7b. Then from 30 to 365 days, this ratio steadily decreased from 2.0 to 1.8. This behavior is similar to what was found by Neill et al. for ISG dissolved in the presence of magnetite¹³. This will be

discussed in a later section. The Fe concentration measured for ISG (+SS) in silica-saturated NaCl is much less than that measured in 0.6 M NaCl with no pre-dissolved silica. The final pH values at the end of the experiment were measured to be 7.9 and 8.7 for the silica-saturated and the 0.6 M NaCl solutions, respectively. At such pH values, the solubility of Fe ions is less than in acidic to neutral pH values. Since the precipitation of Fe-Si secondary phases was much less in silica-saturated conditions, the lower amount of dissolved Fe is indicative of a lesser degree of SS crevice corrosion, as was confirmed by microscopy images (Figs. 1, 2). The Equivalent Thickness of the gel layer can be estimated from B release (ET(B)), and this has been compared with the gel thickness measured with SEM (Supplementary Fig. 2). Again, the 30 day data are from Guo et al.²¹ These values agree reasonably well at 182 days and 365 days for ISG(+SS) reacted in 0.6 M NaCl. The larger difference between the ET(B) value and the gel thickness measured by SEM at 30 days (Supplementary Fig. 2a) is likely associated with the highly heterogenous alteration observed at this stage²¹. For silicasaturated NaCl, there is reasonable agreement between the two values except at 365 days.

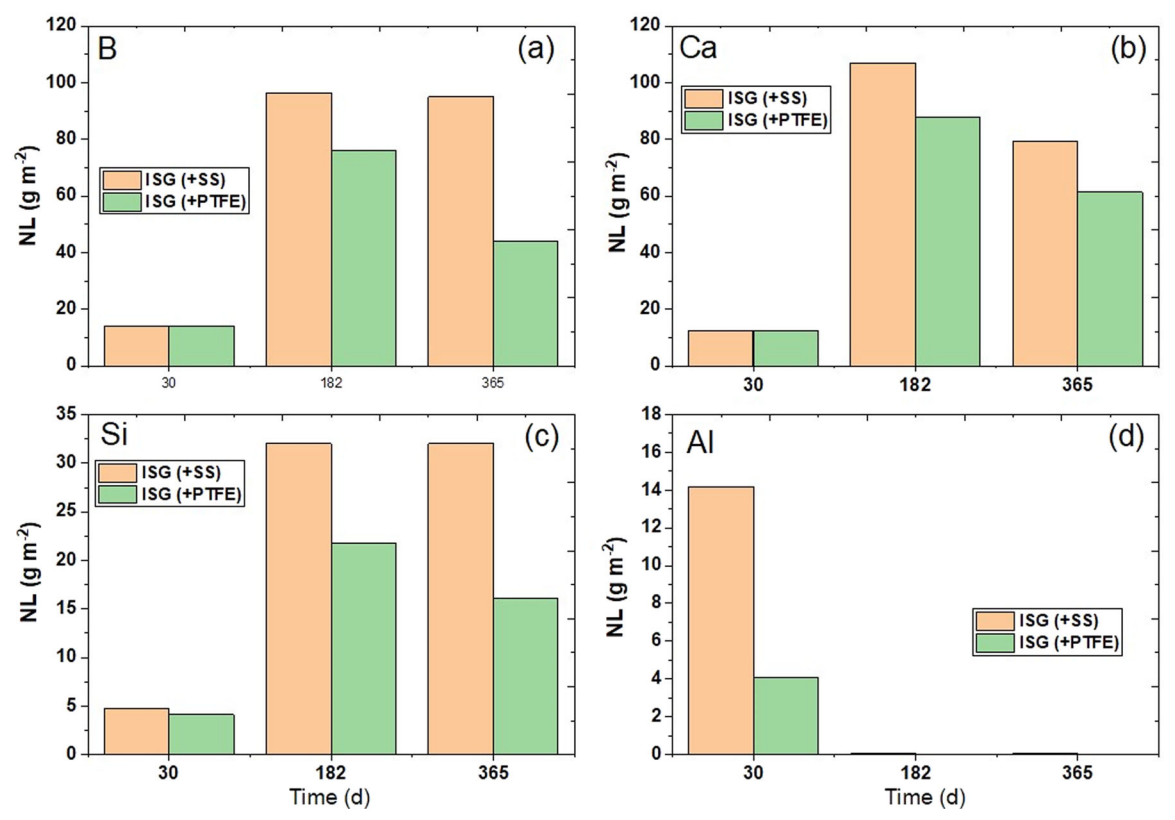


Fig. 6 Normalized loss (NL) (in g/m2) of glass constituent elements from ISG(+SS) and ISG(+PTFE) dissolution in 0.6 M NaCl. (a) B (b) Ca. (c) Si (d) Al. Zr concentration was below detection limit. For ISG(+PTFE), Al concentration was below detection limit. The data at 30 days from Guo et. al²¹. have been added for reference. Note that for Ca, the 30 day data points for ISG(+PTFE) and ISG (+SS) are the same. The contact area between ISG and SS and ISG and PTFE has been included for these data. The concentration of Al at 182 days and 365 days for ISG(+PTFE) were below detection limit of the instrument.

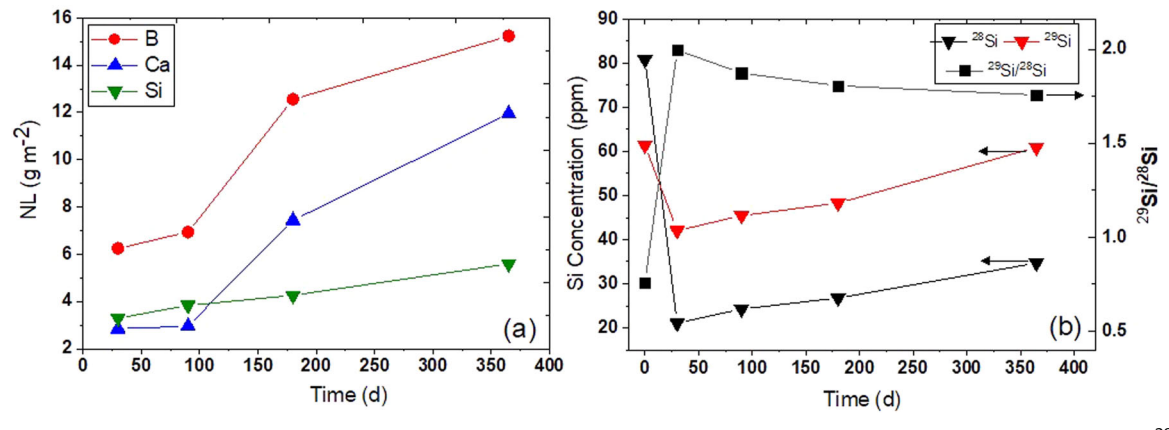


Fig. 7 Solution analyses data from ISG(+SS) dissolution in silica-saturated NaCl. a NL for B, Si and Ca. b The concentrations of ²⁸Si and ²⁹Si measured by ICP-MS and the ²⁹Si/²⁸Si isotopic ratio in the bulk solution. The contact area between ISG and SS and ISG and PTFE has been included for these data.

Specular Reflectance Infrared Spectroscopy (SR-IR)

The changes in the silicate bonding environment of the gel were examined by SR-IR measurements at different locations of the corroded ISG. The data are presented in Fig. 8. The region of interest is from 800 cm^{-1} to 1600 cm^{-1} as this encompasses the vibrational modes corresponding to the local structures of the aluminosilicate network³¹. Fig. 8a shows the SR-IR spectra acquired for ISG(+SS) exposed in 0.6 M NaCl. Spectra were taken at locations 1 through 5 where 1 lies outside the crevice and 2 through 5 lie in the crevice, as shown in Fig. 8a'. Also included are

spectra corresponding to pristine ISG and pure vitreous silica, v-SiO₂, for comparison. We observed the $1038\,\mathrm{cm}^{-1}$ band corresponding to the asymmetric Si-O-Si(B,AI) stretch mode (u_{as}) in ISG $^{32-34}$.

For region 1, this band has been red-shifted by 38 cm⁻¹, and for region 4 this band has blue-shifted by ~30 cm⁻¹. If this blue-shift is compared with the empirical relationship found for the bond length distribution of silica and silicate glasses²⁷, it would correspond to a decrease of average Si-O bond length by ~0.01 Å. Recall that the local solution pH is alkaline outside the



Table 2. Re	Table 2. Results of solution analyses for ISG-SS dissolution in silica-saturated NaCl.								
ICP-MS solution analyses results for ISG(+SS) dissolution in silica-saturated NaCl									
Time (d)	²⁸ Si	²⁹ Si	Al	Fe	В	Ca	²⁹ Si/ ²⁸ Si	Eth(B) * (μm)	Eth(B) ** (μm)
0	80.8	61.4	-	-	-	-	0.76		
30	21.08	42.05	0.008	0.001	7.76	2.76	1.99	1.7	2.7
90	24.28	45.44	0.007	0.08	8.61	2.85	1.87	1.9	3.0
182	26.76	48.29	0.009	0.09	15.41	6.48	1.80	3.4	5.3
365	34.68	60.88	0.013	0.13	18.67	10.12	1.76	4.1	6.4

All numbers are in ppm. The equivalent thickness ET(B) was estimated by including the ISG (+SS) contact area in the SA/V (ET(B)*) and excluding the ISG(+SS) contact area in the SA/V (ET(B)**).

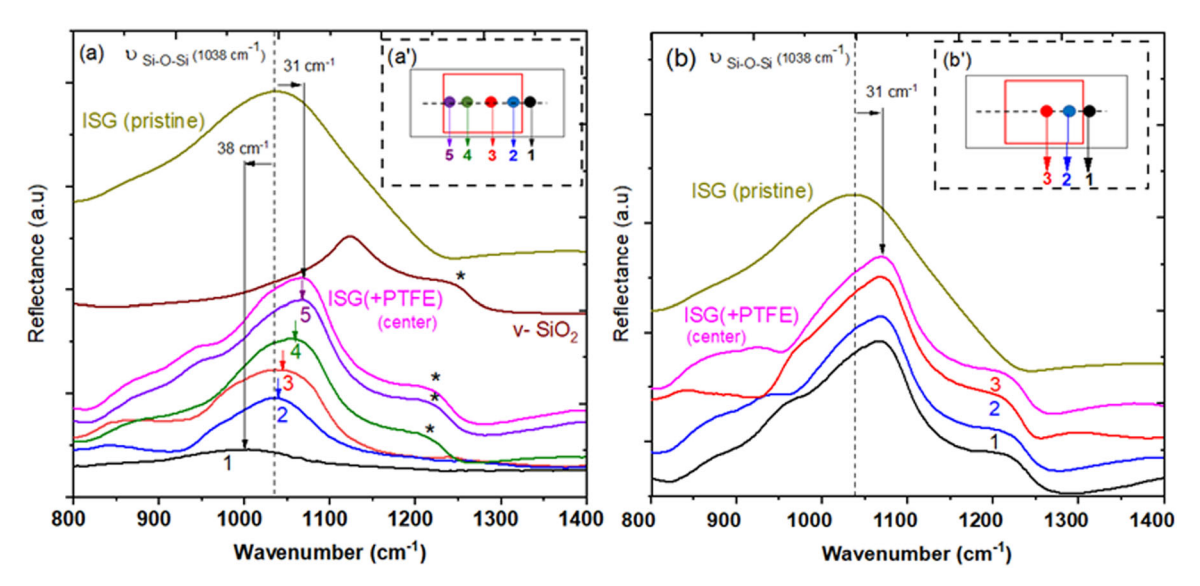


Fig. 8 SR-IR results displayed as reflectance acquired on ISG(+SS) samples. a) Reflectance data for spots 1 through 5 for ISG(+SS) in 0.6 M NaCl along with a spectrum of pristine ISG and glassy SiO₂. a') An illustration of the ISG(+SS) sample with numbers indicating the spots where spectra were acquired. The smaller rectangle in red represents the contact area of ISG with SS. A spectrum of an ISG(+PTFE) sample acquired at the geometric center of the sample is also included for comparison (in magenta color). Notably, spots 2 and 3 correspond to the vicinity of the large pits observed on the SS sample. **b)** Reflectance data for spots 1 through 3 for ISG(+SS) in silica-saturated 0.6 M NaCl along with a spectrum of pristine ISG and a spectrum of ISG(+PTFE) for the same solution. b') An illustration of the ISG(+SS) sample with numbers indicating the spots where spectra were acquired and the smaller rectangle in red representing the contact region with SS.

crevice owing to the predominance of the cathodic oxygen reduction reaction on the SS surface. A higher pH can facilitate Si-O hydrolysis^{35,36} and cause the gel to be deficient in Si with a concomitant presence of a large quantify of Si species with more NBO groups. Therefore, the red-shift of the u_{as} mode may be caused by a decrease in the average force constant of the Si-O bond^{37,38}. The force constant of a bond may be thought of as a restoring force on a bond if it is displaced by a unit distance and reflects the strength of a bond 32,37. A decrease in bond length has been correlated with an increase in the force constant 39,40. Inside the crevice region, due to an expected neutral to acidic pH, the mobile elements are released from the glass more readily, leaving behind a gel structure enriched with silica components. The full width half maximum (FWHM) for this peak decreases measurably compared to that of ISG, signifying a narrower bond parameter distribution of the silicate network in the gel41,42. Furthermore, a shoulder appeared at ~1200 cm⁻¹ (marked by *), which is characteristic of the Si-O-Si network (as in v-SiO₂)⁴³.

Regions 2 and 3 correspond to the vicinity of the large pits observed on the SS sample (Fig. 1a-f) and thus would have contacted an environment with relatively large amounts of Fe

ions. For regions 2 and 3, the relative blue-shift of v_{as} with respect to ISG is $7 \, \text{cm}^{-1}$ and $3 \, \text{cm}^{-1}$, respectively, Fig. 9c. Interestingly, these two spectra do not exhibit the $1200 \, \text{cm}^{-1}$ shoulder characteristic of the Si-O-Si network, which probably is because of SS dissolution on the gel structure at these locations, but the detailed mechanism needs further investigation. Note that, as seen in Fig. 4a at spots 4 and 5, localized damage on ISG was not observed. In comparison, the spectrum for a control sample (ISG (+PTFE)) taken at the center of the sample (Fig. 8a), exhibits a $31 \, \text{cm}^{-1}$ blue-shift for the v_{as} mode and shows the $1200 \, \text{cm}^{-1}$ peak. The comparison of the spectra of regions 2 and 3 with the ISG(+PTFE) control spectrum suggests that SS cations like Fe²⁺ and Fe³⁺ may impede structural reorganization of the gel¹⁷.

Three locations were tested for the sample exposed in SiO_2 —saturated solution, as shown in Fig. 8b'. The u_{as} mode blue-shifted by 31 cm⁻¹ and the 1200 cm⁻¹ mode is prominently observed at all locations. The small differences in the 850–950 cm⁻¹ region could be due to optical inference from the IR beams reflected from the top and bottom of the alteration layer, especially when the IR penetration depth is comparable to or larger than the alteration layer thickness²⁷. Such interference

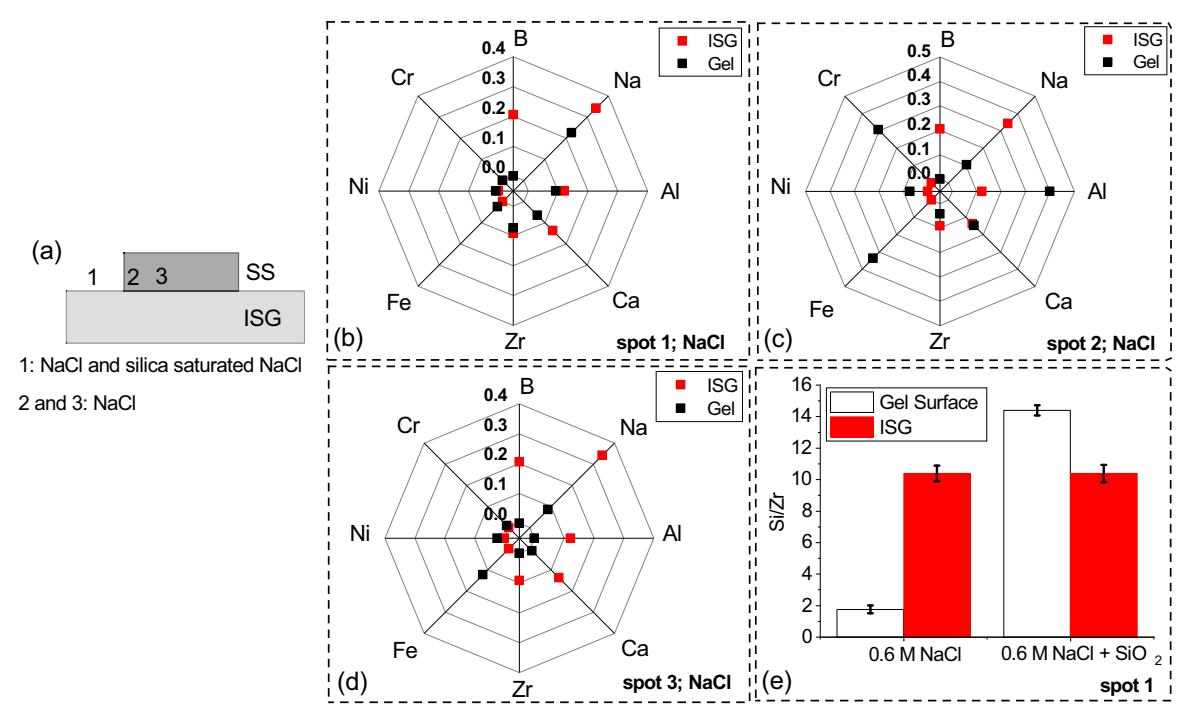


Fig. 9 Results of gel surface chemistry in terms of weight percent of elements obtained with XPS on glass gels and compared with pristine ISG. a) An illustration of the ISG(+SS) creviced assembly where the numbers 1, 2 and 3 represent the spots at which XPS data were acquired. For spot 1, data were collected for ISG samples corroded in NaCl as well in silica-saturated NaCl. For spots 2 and 3, the data were collected only for NaCl solution. Note that spot 3 is closer to the crevice mouth than the crevice center. **b**–**d**) The elemental composition of gel surface normalized to that of Si at regions 1, 2 and 3 in 0.6 M NaCl, respectively. **e**) The weight percent of Si normalized to that of Zr for gel surface at spot 1 for NaCl as well as silica saturated NaCl compared with that of uncorroded ISG.

effects are negligible in the main ν_{as} band region since the alteration layer is thicker than the IR attenuation depth.

Gel surface chemistry

XPS was used to measure the compositional change of elements in the topmost gel layer (~10 nm) of the glass samples exposed to the crevice corrosion conditions, Fig. 9, in which all compositions were normalized to that of Si. For the ISG(+SS) samples exposed in 0.6 M NaCl, data were acquired at 3 different locations (spots 1, 2 and 3 in Fig. 9a). A low concentration of Fe was detected in region 1 corresponding to the area exposed to the bulk solution (Fig. 9b), which is probably the consequence of Fe²⁺ and Fe³⁻ being transported out of the crevice and then depositing on the glass surface near the external surface of the SS where the local pH was high. The high concentration of Na remaining in the gel at location 1 is associated with the high concentration of Na⁺ existing in the leaching solution. At spot 2 corresponding to the crevice mouth (Fig. 9c), a significant enrichment of Fe and Cr is seen, and a finite amount of Ni is also detected. These elements all originated from the localized corrosion of SS and subsequently precipitated in this area. A higher amount of Al is also observed compared to pristine ISG, possibly due to precipitation of Alcontaining compounds. In region 3, which was located within the crevice and approximately 1.5 mm away from the crevice mouth (Fig. 9d), no Al and Zr were detected on the surface and the Ca concentration was also low. The acidity at spot 3 was likely higher than that of region 2 and it was possibly enough to prevent the precipitation of Al-, Zr- and Ca-containing species. The highly acidic environment may have also prevented the precipitation of secondary phases in this area, so the dissolved species such as Fe²⁺, Cr³⁺, Ni²⁺, Al³⁺, and Ca²⁺ had to transport to spot 2 near the crevice mouth, leading to the evident precipitation identified in Fig. 9c. Interestingly, this region (spot 3) within the crevice correlates with the observation of etch pits on the ISG(+SS)

sample, which in turn correlates with the SS corrosion observed in Fig. 1. This observation is consistent with the classical crevice corrosion theory, where a high concentration of metal cations is generated within a confined space due to the anodic dissolution of metal within the crevice 44,45. The dissolved cations subsequently transport toward the bulk solution and then precipitate as the solution pH increases along the diffusion path. The chemistry of the altered surface at region 1 was also evaluated in terms of Si/ Zr ratio (Fig. 9e) since Zr is not expected to dissolve in a mildly alkaline pH range^{22,46}. In 0.6 M NaCl, the Si/Zr ratio on the gel surface is 1.8 as compared to 10.4 on the pristine ISG, a retention of ~17% of Si in the gel. One may correlate this to the alkaline pH outside the crevice due to the oxygen reduction reaction because it is known that a high pH facilitates Si-O dissolution. This certainly validates the red-shifting of the v_{as} mode as seen in the SRIR spectrum in Fig. 8a. For the silica-saturated solution, this ratio is larger than that for ISG, indicating enrichment of Si in the altered surface compared to the pristine ISG (Fig. 9e). This enrichment is manifested in the blue-shifting of the vas mode owing to a SiO2enriched gel. In the NaCl solution without pre-saturated silica, the Si depletion observed through XPS and the resultant red-shift of the u_{as} mode correlate with the degree of SS corrosion. This in turn correlates with a higher pH outside the crevice in 0.6 M NaCl than in the silica-saturated solution because the higher anodic dissolution (metal oxidation) in the crevice must be coupled with enhanced oxygen reduction reaction in the bulk, which leads to more hydroxyl ions and a higher pH. For silica-saturated NaCl, data were acquired at locations 1 and 3* due to difficulty in visually discerning a clear boundary (spot 2) of the crevice mouth on the corroded glass surface. These data, shown in Supplementary Fig. 3, indicate a higher amount of Al- and Ca-containing species compared to that observed in NaCl solution (Fig. 9d). The Fe detected on the altered surface is probably in the form of secondary phase precipitates.



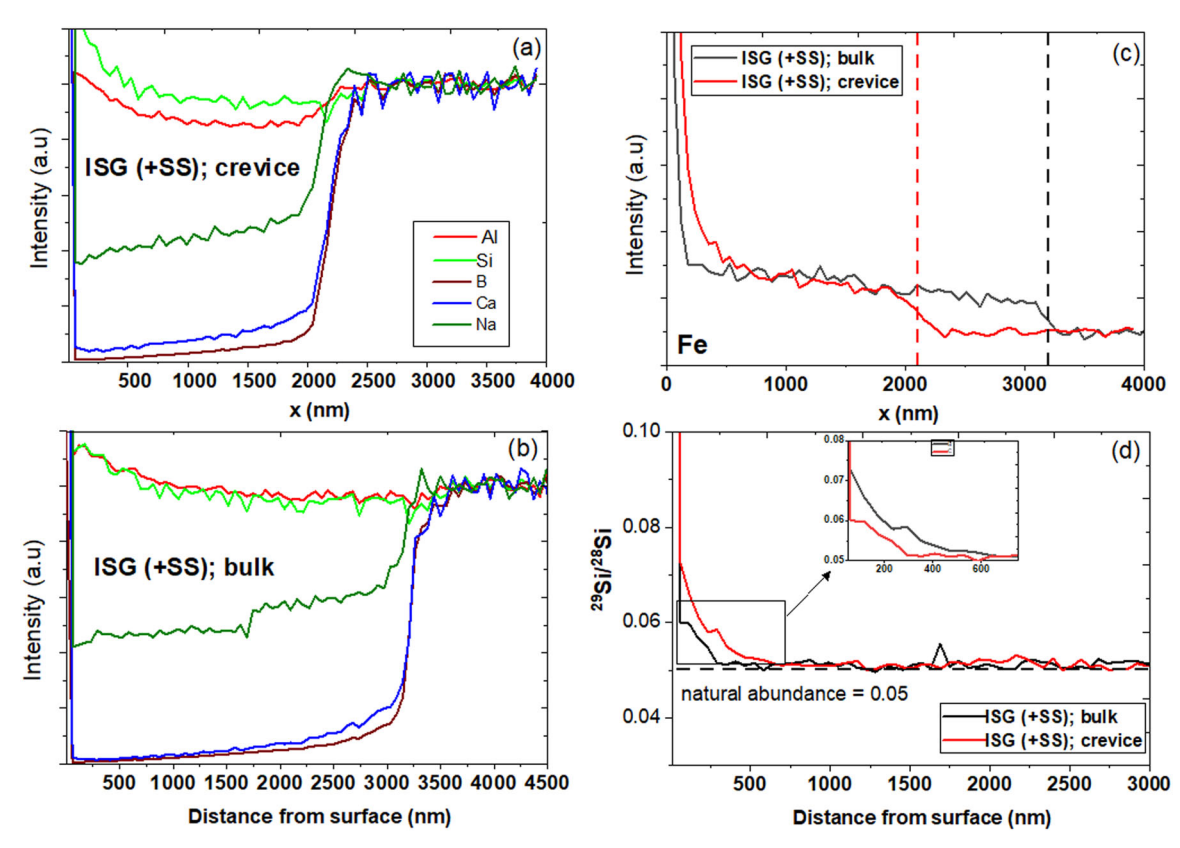


Fig. 10 ToF-SIMS elemental profiling performed on ISG(+SS) in silica-saturated NaCl. a) The depth profiles of glass constituents on the ISG (+SS) creviced region. **b)** corresponding data for the ISG(+SS) bulk region. **c)** The depth profile of Fe in both the creviced region and the bulk. The data for Cr and Ni suffer from too large noise and hence have not been reproduced here. **d)** 29 Si/ 28 Si profile on ISG(+SS) in both creviced region and the bulk.

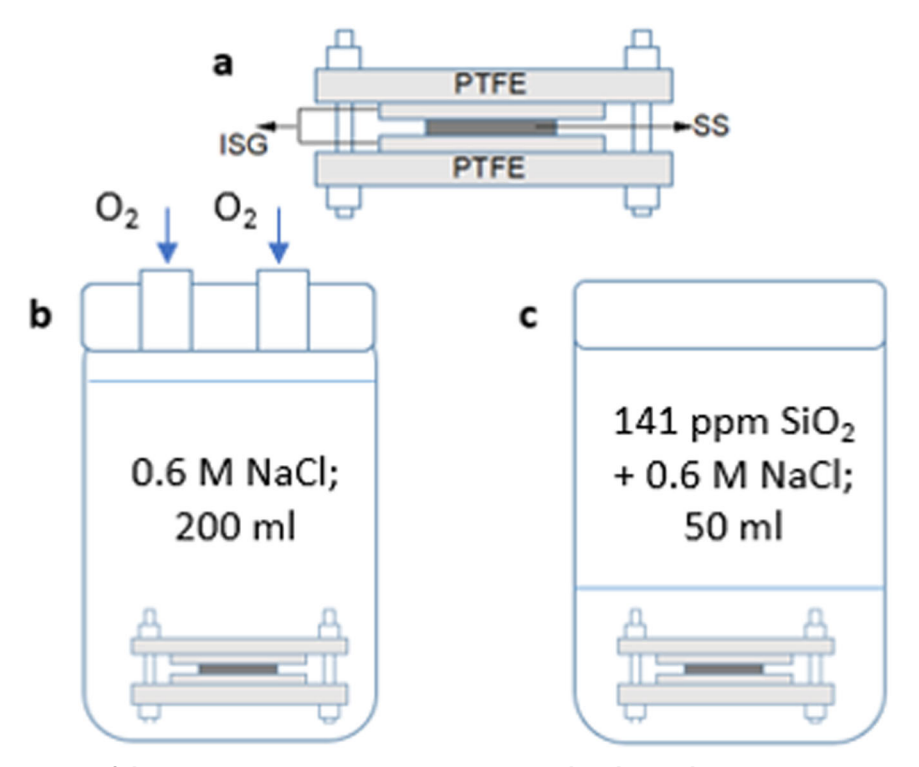


Fig. 11 A schematic illustration of the crevice corrosion experiment setup used in this study. a A SS coupon is sandwiched between two ISG coupons. PTFE plates are placed on the ISG coupons and intimate contact is established with PTFE nuts and bolts. This assembly of samples is then placed in PFA jars. b An illustration of the jar used for 0.6 M NaCl solution. c An illustration of the jar used for silica saturated 0.6 M NaCl.

Time Of Flight SIMS (ToF-SIMS) elemental depth profiling

ToF-SIMS profiling was performed on an ISG(+SS) coupon reacted in silica-saturated 0.6 M NaCl at the center of the crevice (Fig. 10a) and at a location exposed to the bulk solution, about 12 mm from the center (Fig. 10b). For both regions, the depth profiles are qualitatively the same. However, the gel thickness in the crevice is 2100 nm whereas it is 3200 nm in the bulk as demarcated by the rise in the B, Ca and Na compositions in Fig. 10a, b. The sigmoidal profiles in Na and Ca are due to loss of these elements by ionexchange, whereas the sigmoidal profile of B results from the relative ease of B-O bond hydrolysis, resulting in higher mobility of B. The slightly elevated concentration of Na is likely due to the high concentration (0.6 M) of Na⁺ in the bulk solution, which agrees well with the XPS results (Supplementary Fig. 3). The gel of the bulk solution sample is enriched in Si to ~500 nm into the surface as seen in Fig. 10b. Slight depletion of Al was identified (compared to pristine ISG) for the gel of the crevice sample (Fig. 10a), which is again consistent with the XPS data (Supplementary Fig. 3) and likely due to acidic leaching. Components from SS corrosion (Fe, Ni and Cr) are also retained in the gel. Only the Fe compositional profile has been shown in Fig. 10c because the data for Ni and Cr were very noisy. However, Fe is only enriched in the first few 100 nm of the gel surface, suggesting that its incorporation may be due to coprecipitation of Fe-Si compounds because Si is also enriched in the same depth regime. Fe retention in the gel is slightly higher in the crevice compared to the bulk (Fig. 10c) and this may be a mass-transport effect. The ²⁹Si/²⁸Si ratio drops to natural abundance in the first 500 nm (Fig. 10d). However, ²⁹Si enrichment in the crevice sample is a few percent higher than in the bulk sample. A higher ratio of ²⁹Si/²⁸Si suggests that the gel formed within the crevice is more reactive than that formed on the surface exposed to the bulk solution. The enhanced gel activity within the crevice might be associated with the higher Fe content and/or the reduced Al concentration, both of which were caused by the corrosion of SS. Based on the morphological characterization (Fig. 2), the corrosion of SS was under activation control in silica-saturated solutions. However, it seems that pits/ metastable pits were still forming, which might have altered the physiochemical properties of the gel layer within the crevice. Therefore, an even longer exposure study is required to further examine how these early stages of localized corrosion develop over time and affect the glass gel layer. It is also worth noting that the ²⁹Si/²⁸Si isotopic ratio in the gel is similar to what has been seen in several earlier studies^{24,25,35,47}. The fact that most of the gel layer retained ²⁹Si in natural abundance suggests that the gel may have formed due to in-situ reorganization of the silicate network after the release of mobile elements instead of dissolution/reprecipitation^{24,25,35}.

DISCUSSION

In 0.6 M NaCl bulk solution, the crevice corrosion of SS(+ISG) is severe. Large, coalesced pits could be seen close to the crevice mouth. The crystallographic morphology of the pit bottom indicates that the localized attack is activation controlled⁴⁸. The acidic environment in the crevice creates an aggressive enough environment for dissolution of sparingly soluble elements like Al and Zr⁴⁹ as indicated by the XPS measurements. A low pH is known to facilitate ion exchange reactions resulting in removal of Na and Ca from ISG, along with B dissolution²¹. The blue-shift of the v_{as} mode and a concomitant appearance of a 'shoulder band' at $\sim 1200\,\mathrm{cm}^{-1}$ reminiscent of v-SiO₂ suggests that the gel rearranges to a silica-like network structure. A similar observation was also made in silica-saturated solutions. Outside the SS(+ISG) crevice, the pH is expected to be alkaline due to the oxygen reduction reaction on the SS surface. A higher pH can facilitate the Si-O bond dissolution and the precipitation of secondary phases. The red-shift of the v_{as} mode in the SR-IR spectrum acquired outside the creviced region suggests that the gel is Si-deficient. In under-saturated conditions, more alteration phases formed on SS outside the SS(+ISG) crevice than in silica-saturated conditions. This correlates with the greater extent of SS localized corrosion in the unsaturated condition. Guo et al²¹. accelerated SS crevice corrosion by potentiodynamically polarizing SS in solutions containing glass corrosion products and observed massive precipitation of secondary phases²¹. It is also well known that dissolved Si species in aqueous CI⁻ solutions may inhibit localized corrosion by preferential adsorption compared to CI⁻ on the SS surface^{50–52}. The most crucial observation appears to be the highly localized attack on ISG(+SS) in 0.6 M NaCl solution. This situation evidently would be harmful to nuclear waste glass in a repository environment where a localized SS canister corrosion could accelerate glass corrosion and prevent the formation of a protective gel.

In the control experiment of SS(+PTFE) in silica-saturated 0.6 M NaCl, the extent of localized corrosion on SS is more than that observed in SS(+ISG) under the same conditions. The silica species dissolved from ISG may provide enough Si to inhibit corrosion on SS. However, the observation of extensive and still propagating pitting corrosion of SS(+ISG) in 0.6 M NaCl indicates that local Si concentration in the crevice solution may not be enough to completely suppress the localized corrosion of SS. Therefore, it can be concluded that a high initial concentration of pre-dissolved silica substantially reduces the corrosion rate of SS. However, when the initial solution does not contain such a high concentration of silica, localized corrosion of SS can still initiate and propagate to a great extent, which subsequently enhances the corrosion of adjacent glass in a highly localized manner. At the proposed Yucca Mountain location under consideration in the US as the site of a permanent repository, the water that might contact the waste package can either come from dripping or condensation so it is highly unlikely that such water will contain silica with a concentration comparable to what was used in this study (141 ppm)⁵³. Therefore, localized corrosion of metallic canister could occur, which may cause enhanced corrosion of nearby glass. Although the silica concentration would increase over time due to the corrosion of glass, the dissolved silica at the metal-glass interface can quickly precipitate, owing primarily to the high affinity of metal cations toward silicate and the much lower dissolution rate of glass than metals.

It is possible that the accumulation of corrosion products at the crevice mouth might clog the crevice and thus suppress the crevice corrosion of SS. However, Figs. 1 and 2 clearly show that, although substantial corrosion products accumulated at the crevice mouth, the degree of localized corrosion on SS unambiguously became more severe compared to the short-term study²². This may be attributed to the widening of the initial crevice gap at the crevice mouth due to the preferential attack of SS and the subsequent transition of preferential corrosion site toward the crevice center. This is supported by the more severe corrosion damage at a location of ~1.5 mm from the crevice mouth on SS (Fig. 1a–c), which corresponds to spot 3 on ISG in Fig. 9d rather than spot 2 in Fig. 9c after 12 months of exposure in 0.6 M NaCl.

In our solution analyses, we observe a decrease in Si concentration by ~80 ppm between 0–30 days of reaction. To account for this decrease, we consider three processes: (i) precipitation of amorphous SiO_2 on the SS surface, (ii) precipitation of Fe-Si secondary phases and (iii) adsorption of Si on the SS surface. These three effects evidently dominate dissolution during the first 30 days of reaction.

Marshall and coworkers 54,55 systematically studied the effect of electrolytes on silica solubility and showed that a 0.6 M NaCl solution at pH 7 decreases silica solubility to \sim 120 ppm compared to \sim 135 ppm in pure water. Therefore, in the present work, the salinity of the solution alone may account for \sim 22 ppm of SiO₂



Table 3. Sorption capacities and specific surface areas of oxides of Fe taken from literature. The surface area for SS samples is 9 cm ² .							
	Maximum Sorption capacity ($\mu mol_{Si} g^{-1}$)	Specific surface area (m ² g ⁻¹)	Mass of oxide formed (g)	Si adsorbed (ppm)			
Hematite	2.03 (14)	67.5 (⁵⁷)	1.3×10^{-5}	5.4 × 10 ⁻⁵			
Magnetite	33 (¹⁵)	2 (¹⁵)	4.5×10^{-4}	0.03			
Goethite	100 (¹⁵)	22 (¹⁵)	4.1×10^{-5}	0.008			
Siderite	28 (¹⁵)	0.47 (15)	0.002	0.11			

0.018

1.26

0.037

precipitation. In the present pH and temperature conditions, the precipitation kinetics of amorphous SiO_2 , considering a pseudofirst order rate law are unlikely to account for the observed ~80 ppm decrease in measured Si concentration because the affinity term (1-Q/K) nearly vanishes at close to equilibrium concentration of silica^{56,57}. Our analyses, SEM-EDS on the SS surface and ToF SIMS on the corroded ISG surface, indicate Fe-Si secondary phase precipitation, controlled by SS dissolution. Because we do not observe severe corrosion on our SS samples in saturated silica conditions, the amount of such precipitates is not sufficient to explain the observed Si consumption.

Adsorption of SiO₂ on the Fe oxide surfaces suppresses the saturation of the solution and results in an enhancement of glass dissolution. The adsorption capacities of Fe oxides studied by Philipini et al. 15 and Jordan et al. 14 have been summarized in Table 3. We utilized published values of specific surface area of Fe oxides, namely hematite (67.5 m $^2g^{-1}$)⁵⁸, magnetite (2 m $^2g^{-1}$)¹⁵, goethite (22 m $^2g^{-1}$)¹⁵ and siderite (0.47 m $^2g^{-1}$)¹⁵. By considering the sample surface area that is available for Si adsorption (9 cm²) and the specific surface area of oxides, we can arrive at the mass of the specific oxide that may form on the sample surface. The amount of Si adsorbed can then be calculated from the adsorption capacities. It can be seen from Table 3 that the amount of Si adsorbed on hematite, magnetite, goethite and siderite are 5.4×10^{-5} ppm, 0.03 ppm, 0.008 ppm and 0.11 ppm, respectively. These values indicate that the effect of adsorption is probably minor. However, silica sorption capacities for oxides of Cr, Ni and Mo are not available to the best of our knowledge. Therefore, it is possible that adsorption of silica on surfaces of stainless steels could be higher. Therefore, we postulate that the SiO₂ consumption between 0-30 days of reaction should be a combined effect of amorphous SiO₂ precipitation, SiO₂ adsorption and secondary phase precipitation. Subsequently, between 30 days and 365 days, the steady increase in the Si concentration is an outcome of preferential ISG dissolution.

The details of how SS metal cations affect the glass gel layer are unknown. It has been suggested that the gel layer porosity may be decreased by clogging of pores through incorporation of cations⁵⁹, thereby leading to slower diffusion of mobile elements into solution. Such an inhibitive effect was not observed in this study because there was clear evidence of Fe incorporation into the first several hundred nm of the gel layer (Fig. 10c). However, the corrosion rate of ISG(+SS) increased slightly compared to ISG (+PTFE) as suggested from the gel layer thickness (Supplementary Fig. 1). Since the solution was silica-saturated, the corrosion rate of SS and subsequently the interaction between SS and ISG was significantly reduced. This makes it more difficult to identify the potential inhibition mechanism. Future studies will focus on using ToF-SIMS to analyze the gel layer formed on ISG(+SS) that was corroded in 0.6 M NaCl for 12 months. It may also be possible that cations like Fe²⁺ and Fe³⁺ can depolymerize the silicate gel network and retard the in-situ reorganization. This may be the case because our SR-IR data show that in the presence of SS the u_{as Si-O-Si} mode red-shifts compared with the control sample, suggesting metal cations can depolymerize the gel network and prevent a complete structural reorganization of the gel. However, further evidence is required. The ToF-SIMS data suggest that the Fe retention in the gel in the ISG(+SS) contact region is a few

Table 4. Chemical composition of ISG and SS316 samples used in this study. a Chemical composition of ISG in weight % of elements Si В Na ΑI Ca Zr 0 26.3 5.4 9.0 3.2 3.6 2.4 50.1 b Chemical composition of SS316 in weight % of elements Co Mn W Cu Si Cr Ni Мо Nb Fe

percent higher than in the non-contact area (Fig. 10c). This is correlated with a slightly higher ²⁹Si retention in the gel due to saturation effects in the crevice solution and/or the enhanced activity of the gel (Fig. 10d).

16.67

10.07

2.01

0.05

Bal

0.27

0.001

Finally, the experimental conditions used in this study may be a reasonable representation of the conditions expected in the planned repository in the U.S. This work suggests that localized corrosion of SS canisters might aggravate vitrified nuclear waste glass dissolution. However, it must be emphasized that, although a global acceleration of corrosion exists as supported by the solid and solution analysis data, the effect of SS corrosion on glass alteration is highly localized. The local damage on the gel might cause stress concentration on the glass surface and affect the integrity of the glass substrate, which should be a topic of future study. In addition, the gel layer on the glass exposed to the bulk solution showed substantial cracks. These effects ought to be incorporated in the long-term predictability and performance modeling of waste forms.

The following is a summary of our key findings.

- (a) Severe SS crevice corrosion in 0.6 M NaCl solution increases ISG dissolution with an enhancement in silicate network dissolution observed in the alkaline pH conditions on the SS cathode (exposed to bulk solution) and enhancement in ion-exchange reactions at the anode (contact region). The highly acidic conditions resulting from SS cation hydrolysis causes the removal of Zr and Al and results in an "etched" attack on ISG.
- (b) Secondary phase precipitation correlates with the degree of SS crevice corrosion and is much more intense in Si unsaturated 0.6 M NaCl. The pre-dissolved silica and ISG corrosion combine to inhibit SS crevice corrosion.
- (c) The solution analyses results in silica-saturated solution suggest that both adsorption and precipitation of amorphous silica and secondary silicate phases provide the driving force for ISG dissolution.

METHODS

Materials and sample preparation

The ISG samples used in this study were provided by Pacific Northwest National Laboratory and Savanah River National Laboratory. The chemical compositions of ISG and SS 316 are given in Table 4. All water used in this study was deionized (DI) water with resistivity of 18.2 $M\Omega \cdot cm$. The ISG

coupons with a dimension of (25 mm × 11 mm × 3 mm) were machined from the as-received ISG blocks. The SS sheet was cut into 25 mm \times 25 mm × 3 mm specimens. Prior to corrosion experiments, the SS and ISG samples were abraded to 1200 grit using SiC paper, degreased in ethanol by ultrasonic cleaning and rinsed and dried. The average roughness of the ISG samples was 0.05 µm. Prior to assembling the coupons for crevice corrosion, the contact area between ISG and SS was wetted with the electrolyte. 0.6 M NaCl solution was prepared by dissolving the required amount of NaCl (crystalline/certified ACS; Fischer Scientific) in deionized (DI) water. Saturated SiO₂ solution was prepared by adding amorphous ²⁹SiO₂ and ²⁸SiO₂ powders (2:1) into DI water. The solution pH was first adjusted to 11.5 using 0.1 M LiOH and 0.1 M HNO₃ to facilitate the dissolution of SiO₂. The solution was periodically analyzed by Inductively Coupled Plasma Mass Spectrometry (ICP-MS) until the concentration of SiO₂ reached saturation (~140 ppm)¹³. Upon confirmation of solution saturation with regard to SiO₂ after 6 months, the solution pH was adjusted back to neutral and NaCl salt was added to reach a concentration of 0.6 M.

Corrosion experiments

The ISG(+SS), corrosion experiments were performed by placing a coupon of SS 316 in intimate contact sandwiched between two ISG coupons as shown in Fig. 11. For the ISG(+PTFE) corrosion experiment, a coupon of PTFE was sandwiched in intimate contact between two ISG coupons. For the SS(+PTFE) corrosion experiment, a coupon of SS was sandwiched in intimate contact between two PTFE coupons.

PTFE plates were used to sandwich the ISG, and SS coupons and tight contact was established by PTFE nuts and bolts. This setup ensures that crevice corrosion only occurs at the interfaces of SS and ISG (for the experimental group), or SS and PTFE (for the control group). The entire assembly was placed in a perfluoroalkoxy alkane (PFA) jar containing the electrolyte. For each sample of sandwiched ISG-SS-ISG (a SS 316 coupon sandwiched between a pair of ISG coupons), controls of ISG-PTFE-ISG and PTFE-SS-PTFE were also made for each testing solution. For solution containing dissolved SiO₂, the solution volume was kept at 50 ml whereas, for the solution with no dissolved SiO₂, a volume of 200 ml was used. It was expected that under SiO₂-containing conditions, the residual rate of dissolution would be attained quicker and concomitantly a gel layer would form earlier in the smaller volume of solution. Therefore, a higher SA/V ratio was used in the solution containing SiO₂. Since no O₂ could enter this reaction vessel, the lids of this vessel were opened every two days to replenish the reaction vessel with ambient air. All PFA vessels containing reacting samples were placed in a water bath, where the temperature was maintained at 90 ± 1 °C. After the exposure duration, the vessels were removed from the water bath, and the solution was collected for chemical composition analyses using Inductively Coupled Plasma - Optical Emission Spectrometry (ICP-OES) and ICP-mass spectroscopy (ICP-MS) for silicasaturated NaCl solutions. The sample assemblies were removed and dismantled. All coupons were rinsed with DI water for a few minutes and air dried. The samples were then wrapped in Al foil and stored for future characterization. One ISG coupon and one SS coupon from an ISG-SS assembly were briefly rinsed, immediately mounted in epoxy by placing them in contact with each other with their faces perpendicular to each other but without being dried, and cross-sectioned for SEM studies by slicing the SS along its width and ISG along its length.

Scanning electron microscopy and energy-dispersive X-ray spectroscopy

The corroded surfaces of SS as well as the cross-sectioned samples were examined by a Thermo Fischer Scientific Apreo FEG SEM containing an Energy Dispersive X-ray Spectroscopy (EDAX) octane Elect EDS System (AMEKET). The cross-sectioned samples were examined to reveal the gel morphology. The cross-sectioned SS-ISG samples and ISG samples were gold sputtered prior to SEM. No such treatment was done for SS samples. The cross-sectioned samples were abraded to 1200 grit SiC paper and rinsed and dried before sputter deposition of Au. Note that all images were acquired in secondary electron mode. Cross-section morphologies in Fig. 5 and Supplementary Fig. 1 were acquired in secondary electron mode with a T1 detector. All other SEM images were acquired with an Everhart Thornley Detector (ETD). The gel thicknesses were measured with ImageJ software. For reliability, measurements were done at 10 locations on a single image.

X-ray photoelectron spectroscopy

All corroded ISG(+SS) samples were characterized by a Kratos XPS system using a monochromatic Al-K α X-ray source. The calibration for all spectra was done with reference to adventitious aliphatic carbon (C-C) at a binding energy (BE) of 284.8 eV. The scanned area for these measurements was approximately 400 \times 600 μ m². For ISG coupons corroded in 0.6 M NaCl with no dissolved SiO₂, data were acquired at 3 different locations viz. surface exposed to bulk solution, at the mouth of the ISG(+SS) crevice and at the center of the crevice region between ISG and SS. For the ISG samples corroded in SiO₂-containing solutions, the data were acquired in the bulk and in the crevice region only. All compositions were normalized to that of Si.

Specular reflectance infrared spectroscopy

SR-IR measurements were made using a Bruker Hyperion 3000 FT-IR spectrometer equipped with a $15\times$ reflective objective. The incidence angle could be varied between $11.3^{\circ}-23.6^{\circ}$ and an aperture of $100\times100~\mu m^2$ was used. A spectrum of gold was used as a reference. Spectra were obtained by averaging 400 scans with a resolution of 6 cm $^{-1}$. For ISG(+SS) samples corroded with no dissolved SiO $_2$ in solution, data were acquired at 5 locations. Location 1 is located just outside the crevice and locations 2, 3, 4 and 5 are all located along the dashed line as shown in Fig. 8a'. For samples corroded in SiO $_2$ -containing solutions, the data were acquired at 3 locations with location 1 being outside the crevice and locations 2 and 3 being inside the crevice along the dashed line as shown in Fig. 8b'.

Time of flight secondary ion mass spectrometry (ToF-SIMS)

ToF SIMS analyses were performed at Tescan Analytics, France by a ToF SIMS5 spectrometer (IONTOF, Munster, Germany). A pulsed 25 KeV \sim 1.5 pA Bi_1^+ ion source was analyzed over an area of $50\times50~\mu m^2$. Depth profiling was performed by abrading the sample surface by O_2^+ ion pulses at KeV and 730 nA over an area of $190\times190~\mu m^2$. Data for all elements were normalized to the Zr concentration.

Solution analyses by ICP and data treatment

The leachates collected were analyzed for elemental concentrations by ICP-OES (Perkin Elmer). For the $\rm SiO_2$ -containing solutions, the analyses were done by ICP-MS due to the presence of $\rm ^{29}Si$ the solution. For each solution analyses, a dilution factor of 200 was used due to the high salinity of the solution. The normalized mass losses of glass, NL, were calculated from the release of various glass constituents using the following relationship:

$$NL_{t}^{i} = \frac{C_{t} - C_{t-1}}{\left(\frac{SA}{V}\right)f^{i}} + NL_{t-1}^{i}$$
(1)

where the subscript and superscript denote the time and element, respectively. C denotes concentration, SA/V denotes the ratio of surface area to solution volume used in the experiment and f denotes the weight fraction of the element that is present in ISG. The equivalent thickness of the alteration layer was estimated from the boron concentration in solution Eth(B) using the following relationship:

$$Eth(B) = \frac{C_B}{\binom{SA}{V}(f_B)(\rho)}$$
 (2)

Where C_B is the concentration of B in the solution, SA/V denotes the ratio of surface area to solution volume used in the experiment and f denotes the weight fraction of B that is present in ISG and ρ is the density of glass ($\rho=2.5~{\rm g/cm^3}$)

DATA AVAILABILITY

The datasets generated during and/or analyzed during the current study are available from the corresponding author on reasonable request.

Received: 4 March 2022; Accepted: 6 May 2022; Published online: 29 June 2022

REFERENCES

 Frankel, G. S. et al. A comparative review of the aqueous corrosion of glasses, crystalline ceramics, and metals. Npj Mater. Degrad. 2, 15 (2018).



- Gin, S. et al. An international initiative on long-term behavior of high-level nuclear waste glass. *Mater. Today* 16, 243–248 (2013).
- Ojovan, M. I., Lee, W. E. & Kalmykov, S. N. An Introduction to Nuclear Waste Immobilisation. (Elsevier. 2019).
- Frankel, G. S. et al. Recent Advances in Corrosion Science Applicable To Disposal of High-Level Nuclear Waste. Chem. Rev. 121, 12327–12383 (2021).
- Vienna, J. D., Ryan, J. V., Gin, S. & Inagaki, Y. Current Understanding and Remaining Challenges in Modeling Long-Term Degradation of Borosilicate Nuclear Waste Glasses. Int. J. Appl. Glass Sci. 4, 283–294 (2013).
- Gin, S., Delaye, J.-M., Angeli, F. & Schuller, S. Aqueous alteration of silicate glass: state of knowledge and perspectives. Npj Mater. Degrad. 5, 1–20 (2021).
- Geisler, T. et al. The mechanism of borosilicate glass corrosion revisited. Geochim. Cosmochim. Acta 158, 112–129 (2015).
- 8. Gin, S. et al. A General Mechanism for Gel Layer Formation on Borosilicate Glass under Aqueous Corrosion. *J. Phys. Chem. C.* **124**, 5132–5144 (2020).
- 9. Lutze, W. & Grambow, B. The effect of glass corrosion on near field chemistry.

 Radiochim Acta 58, 3–8 (1992)
- Guo, X., Gin, S. & Frankel, G. S. Review of corrosion interactions between different materials relevant to disposal of high-level nuclear waste. *Npj Mater. Degrad.* 4, 34 (2020).
- McVay, G. L. & Buckwalter, C. Q. Effect of Iron on Waste-Glass Leaching. J. Am. Ceram. Soc. 66, 170–174 (1983).
- 12. Carriere, C. et al. The fate of Si and Fe while nuclear glass alters with steel and clay. *Npj Mater. Degrad.* **5**, 1–12 (2021).
- Neill, L. et al. Various effects of magnetite on international simple glass (ISG) dissolution: implications for the long-term durability of nuclear glasses. Npj Mater. Degrad. 1, 1 (2017).
- Jordan, N., Marmier, N., Lomenech, C., Giffaut, E. & Ehrhardt, J.-J. Sorption of silicates on goethite, hematite, and magnetite: Experiments and modelling. J. Colloid Interface Sci. 312, 224–229 (2007).
- Philippini, V., Naveau, A., Catalette, H. & Leclercq, S. Sorption of silicon on magnetite and other corrosion products of iron. J. Nucl. Mater. 348, 60–69 (2006).
- Kim, S. S., Lee, J.-G., Choi, J. K., Lee, G. H. & Chun, K. S. Effects of Metals, Metal Oxides and Metal Hydroxide on the Leaching of Simulated Nuclear Waste Glass. Radiochim. Acta 79, 199–206 (1997).
- Burger, E. et al. Impact of iron on nuclear glass alteration in geological repository conditions: A multiscale approach. Appl. Geochem. 31, 159–170 (2013).
- Frankel, G. S. & Sridhar, N. Understanding localized corrosion. *Mater. Today* 11, 38–44 (2008).
- Woodland, A. B., Bates, J. K. & Gerding, T. J. Parametric effects on glass reaction in the unsaturated test method. http://inis.iaea.org/Search/search.aspx?orig_q=RN:23054693 (1991).
- Pan, Y.-M., Jain, V. & Pensado, O. Degradation of high-level waste glass under simulated repository conditions. J. Non-Cryst. Solids 319, 74–88 (2003).
- Guo, X. et al. Near-field corrosion interactions between glass and corrosion resistant alloys. Npj Mater. Degrad. 4, 10 (2020).
- Guo, X. et al. Self-accelerated corrosion of nuclear waste forms at material interfaces. Nat. Mater. 19, 310–316 (2020).
- Farfan-Cabrera, L. I. et al. A crevice corrosion assessment method for joints of mechanical components sealed with composite structure gaskets – The case of the engine cylinder head/mono-block joint. Eng. Fail. Anal. 119, 104981 (2021).
- Gin, S. et al. Dynamics of self-reorganization explains passivation of silicate glasses. Nat. Commun. 9, 2169 (2018).
- Gin, S. et al. Origin and consequences of silicate glass passivation by surface layers. Nat. Commun. 6, 6360 (2015).
- Kaspar, T. C., Reiser, J. T., Ryan, J. V. & Wall, N. A. Non-destructive characterization of corroded glass surfaces by spectroscopic ellipsometry. J. Non-Cryst. Solids 481, 260–266 (2018).
- Kaya, H., Ngo, D., Smith, N. J., Gin, S. & Kim, S. H. Network structure in alteration layer of boroaluminosilicate glass formed by aqueous corrosion. *J. Non-Cryst.* Solids 553, 120494 (2021).
- Dillmann, P., Gin, S., Neff, D., Gentaz, L. & Rebiscoul, D. Effect of natural and synthetic iron corrosion products on silicate glass alteration processes. *Geochim. Cosmochim. Acta* 172, 287–305 (2016).
- Van Eynde, E., Mendez, J. C., Hiemstra, T. & Comans, R. N. J. Boron Adsorption to Ferrihydrite with Implications for Surface Speciation in Soils: Experiments and Modeling. ACS Earth Space Chem. 4, 1269–1280 (2020).
- Godon, N., Gin, S., Rebiscoul, D. & Frugier, P. SON68 Glass Alteration Enhanced by Magnetite. Procedia Earth Planet. Sci. 7, 300–303 (2013).
- Luo, J., Smith, N. J., Pantano, C. G. & Kim, S. H. Complex refractive index of silica, silicate, borosilicate, and boroaluminosilicate glasses – Analysis of glass network vibration modes with specular-reflection IR spectroscopy. J. Non-Cryst. Solids 494, 94–103 (2018).
- 32. Luo, J., Zhou, Y., Milner, S. T., Pantano, C. G. & Kim, S. H. Molecular dynamics study of correlations between IR peak position and bond parameters of silica and

- silicate glasses: Effects of temperature and stress. J. Am. Ceram. Soc. 101, 178–188 (2018).
- Liu, H. et al. Searching for correlations between vibrational spectral features and structural parameters of silicate glass network. J. Am. Ceram. Soc. 103, 3575–3589 (2020)
- Liu, H., Ngo, D., Ren, M., Du, J. & Kim, S. H. Effects of surface initial condition on aqueous corrosion of glass—A study with a model nuclear waste glass. J. Am. Ceram. Soc. 102, 1652–1664 (2019).
- Gin, S. et al. The fate of silicon during glass corrosion under alkaline conditions: A
 mechanistic and kinetic study with the International Simple Glass. Geochim.
 Cosmochim. Acta 151. 68–85 (2015).
- Gin, S. et al. The controversial role of inter-diffusion in glass alteration. Chem. Geol. 440, 115–123 (2016).
- Luo, J., Zhou, Y., Pantano, C. G. & Kim, S. H. Correlation between IR peak position and bond parameter of silica glass: Molecular dynamics study on fictive temperature (cooling rate) effect. J. Am. Ceram. Soc. 101, 5419–5427 (2018).
- Tomozawa, M., Hong, J.-W. & Ryu, S.-R. Infrared (IR) investigation of the structural changes of silica glasses with fictive temperature. J. Non-Cryst. Solids 351, 1054–1060 (2005).
- Zhao, D.-X., Gong, L.-D. & Yang, Z.-Z. The Relations of Bond Length and Force Constant with the Potential Acting on an Electron in a Molecule. J. Phys. Chem. A 109, 10121–10128 (2005).
- 40. Smith, R. P. The Relationship of Force Constant and Bond Length. J. Phys. Chem. 60, 1293–1296 (1956).
- Innocenzi, P. Infrared spectroscopy of sol-gel derived silica-based films: a spectra-microstructure overview. J. Non-Cryst. Solids 316, 309–319 (2003).
- Baral, K., Li, A. & Ching, W.-Y. Ab Initio Study of Hydrolysis Effects in Single and Ion-Exchanged Alkali Aluminosilicate Glasses. J. Phys. Chem. B 124, 8418–8433 (2020).
- Guiton, T. A. & Pantano, C. G. Infrared reflectance spectroscopy of porous silicas. Colloids Surf. Physicochem. Eng. Asp. 74, 33–46 (1993).
- Oldfield, J. W. & Sutton, W. H. Crevice Corrosion of Stainless Steels: I. A Mathematical Model. *Br. Corros. J.* 13, 13–22 (1978).
- Oldfield, J. W. & Sutton, W. H. Crevice Corrosion of Stainless Steels: II. Experimental studies. Br. Corros. J. 13, 104–111 (1978).
- Qiu, L., Guzonas, D. A. & Webb, D. G. Zirconium Dioxide Solubility in High Temperature Aqueous Solutions. J. Solut. Chem. 38, 857–867 (2009).
- Gin, S. et al. Atom-Probe Tomography, TEM and ToF-SIMS study of borosilicate glass alteration rim: A multiscale approach to investigating rate-limiting mechanisms. Geochim. Cosmochim. Acta 202. 57–76 (2017).
- Laycock, N. J. & Newman, R. C. Localised dissolution kinetics, salt films and pitting potentials. Corros. Sci. 39, 1771–1790 (1997).
- Geisler, T. et al. Aqueous corrosion of borosilicate glass under acidic conditions: A new corrosion mechanism. J. Non-Cryst. Solids 356, 1458–1465 (2010).
- Amaral, S. T. & Muller, I. L. Effect of Silicate on Passive Films Anodically Formed on Iron in Alkaline Solution as Studied by Electrochemical Impedance. Spectrosc. Corros. Houst. 55, 17–23 (1999).
- Gao, H. et al. Study of the corrosion inhibition effect of sodium silicate on AZ91D magnesium alloy. Corros. Sci. 53, 1401–1407 (2011).
- Munis, A., Zheng, M. & Zhao, T. Effect of sulfate and meta-silicate ions on pitting corrosion of stainless steel-316 in chloride containing simulated coal gasifier aqueous effluents. *Mater. Res. Express* 6, 076541 (2019).
- Kerrisk, J. F. Groundwater chemistry at Yucca Mountain, Nevada, and vicinity. LA-10929-MS, 60103 http://www.osti.gov/servlets/purl/60103-AN2m45/ (1987) https://doi.org/10.2172/60103.
- Marshall, W. L. & Warakomski, J. M. Amorphous silica solubilities—II. Effect of aqueous salt solutions at 25 °C. Geochim. Cosmochim. Acta 44, 915–924 (1980).
- Marshall, W. L. Amorphous silica solubilities—III. Activity coefficient relations and predictions of solubility behavior in salt solutions, 0–350 °C. Geochim. Cosmochim. Acta 44, 925–931 (1980).
- Rimstidt, J. D. & Barnes, H. L. The kinetics of silica-water reactions. Geochim. Cosmochim. Acta 44, 1683–1699 (1980).
- Carroll, S., Mroczek, E., Alai, M. & Ebert, M. Amorphous silica precipitation (60 to 120 °C): comparison of laboratory and field rates. *Geochim. Cosmochim. Acta* 62, 1379–1396 (1998).
- Jarlbring, M., Gunneriusson, L., Hussmann, B. & Forsling, W. Surface complex characteristics of synthetic maghemite and hematite in aqueous suspensions. J. Colloid Interface Sci. 285, 212–217 (2005).
- Michelin, A. et al. Investigation at the nanometre scale on the corrosion mechanisms of archaeological ferrous artefacts by STXM. J. Anal. Spectrom. 28, 59–66 (2013).

ACKNOWLEDGEMENTS

This work was supported as part of the Center for Performance and Design of Nuclear Waste Forms and Containers, an Energy Frontier Research Center funded by the U.S. Department of Energy, Office of Science, Basic Energy Sciences under Award



#DESC0016584. The authors would like to thank Dr. John Vienna and Dr. Joseph Ryan from Pacific Northwest National Laboratory for providing the ISG samples. The authors would also like to thank Dr. Yutichai Mueanngern and Dr. Yehia Khalifa from Ohio State University for their assistance with XPS measurement and Elodie Chauvet from Tescan Analytics for conducting ToF SIMS analysis.

AUTHOR CONTRIBUTIONS

X.G. conceived the idea. C.M., X.G., H.K., K.Y., and Z.Z. conducted the experiments and collected and analyzed the data. C.M. and X.G. wrote the manuscript. S.G., S.K., J.L., J.W., and G.S.F. supervised the study.

COMPETING INTERESTS

The authors declare no competing interests.

ADDITIONAL INFORMATION

Supplementary information The online version contains supplementary material available at https://doi.org/10.1038/s41529-022-00262-0.

Correspondence and requests for materials should be addressed to Gerald S. Frankel.

Reprints and permission information is available at http://www.nature.com/reprints

Publisher's note Springer Nature remains neutral with regard to jurisdictional claims in published maps and institutional affiliations.

Open Access This article is licensed under a Creative Commons Attribution 4.0 International License, which permits use, sharing, adaptation, distribution and reproduction in any medium or format, as long as you give appropriate credit to the original author(s) and the source, provide a link to the Creative Commons license, and indicate if changes were made. The images or other third party material in this article are included in the article's Creative Commons license, unless indicated otherwise in a credit line to the material. If material is not included in the

article's Creative Commons license and your intended use is not permitted by statutory regulation or exceeds the permitted use, you will need to obtain permission directly from the copyright holder. To view a copy of this license, visit http://creativecommons.org/licenses/by/4.0/.

© The Author(s) 2022